Letter

Machine-learning-coined noise induces energy-saving synchrony

Jingdong Zhang [1,2,3] Luan Yang [2] Qunxi Zhu [2,4,5,*] Celso Grebogi [3] and Wei Lin [1,2,4,5,†]

[1]*School of Mathematical Sciences, SCMS, and SCAM, Fudan University, Shanghai 200433, China*

[2]*Research Institute of Intelligent Complex Systems, Fudan University, Shanghai 200433, China*

[3]*Institute for Complex Systems and Mathematical Biology, King's College, University of Aberdeen, Aberdeen AB24 3UE, United Kingdom*

[4]*Shanghai Artificial Intelligence Laboratory, Shanghai 200232, China*

[5]*MOE Frontiers Center for Brain Science and State Key Laboratory of Medical Neurobiology, Fudan University, Shanghai 200032, China*

(Received 28 February 2024; revised 22 May 2024; accepted 27 June 2024; published 25 July 2024)

Noise-induced synchronization is a pervasive phenomenon observed in a multitude of natural and engineering systems. Here, we devise a machine learning framework with the aim of devising noise controllers to achieve synchronization in diverse complex physical systems. We find the implicit energy regularization phenomenon of the formulated framework that engenders energy-saving artificial noise and we rigorously elucidate the underlying mechanism driving this phenomenon. We substantiate the practical feasibility and efficacy of this framework by testing it across various representative systems of physical and biological significance, each influenced by distinct constraints reflecting real-world scenarios.

DOI: 10.1103/PhysRevE.110.L012203

Introduction. Noise-induced synchronization is a widespread phenomenon observed in various physical systems, encompassing chaotic to limit-cycle oscillators [1–7]. Among the various paradigms of synchronization, complete synchronization (CS) has been extensively discussed in the presence of noise [8–12]. Since Maritan and Banavar claimed that two chaotic systems subjected to the same and sufficiently strong noise can achieve synchronization [13], the mechanisms of common noise enhancing CS and its variants have been a highly relevant topic [4,14,15]. Apart from the common noise, the impact of uncorrelated and correlated noise on synchronization has garnered research attention recently [16,17].

To reveal the complicated mechanism of noise-induced synchronization, previous work has primarily focused on investigating the local stability of the synchronization manifold [8,18] or on exploring the global stability via analytically designing the Lyapunov function for the synchronization error dynamics [10,19,20]. However, all these methods are system specific and pose challenges in devising energy-saved synchronous noise for more general networked systems [21].

In this Letter, we devise and formulate the artificial-intelligence noise (AIN) synchrony, an inaugural and scalable framework for proficiently devising the noise controllers to attain the CS in diverse physical systems, integrating the stochastic stabilization theory with the machine learning techniques. Indeed, the devised AIN synchrony is not only of mathematical rigorousness, but also applicable to stabilizing the synchronization manifold not only in both local but also in global manners. We illustrate its efficacy and practical feasibility using a wide range of representative systems, including chaotic and networked dynamics of limit-cycle oscillators. The results demonstrate that the machine-learning-coined noise can remarkably achieve energy-saving synchrony, which consumes low energy cost in the control process. We call this phenomenon implicit energy regularization and theoretically uncover the universal mechanism that produces it.

Problem setup and notations. We consider the collective dynamics of coupled oscillators, expressed in a general form as

$$\frac{\mathrm{d}\boldsymbol{x}_i}{\mathrm{d}t} = \boldsymbol{M}_0(\boldsymbol{x}_i, \boldsymbol{\mu}_0) + \sum_{j=1}^{n} A_{ij}\boldsymbol{M}_1(\boldsymbol{x}_i, \boldsymbol{x}_j, \boldsymbol{\mu}_1), \tag{1}$$

where $\boldsymbol{x}_i \in \mathbb{R}^d$ $(i = 1, \ldots, n)$ is the oscillatory state of the ith node, $\boldsymbol{M}_0$ represents the self-dynamics of oscillators and exhibits a (unstable) limit cycle or chaotic attractor, denoted by $\boldsymbol{s}$ and satisfying $\mathrm{d}\boldsymbol{s}/\mathrm{d}t = \boldsymbol{M}_0(\boldsymbol{s}, \boldsymbol{\mu}_0)$, $\boldsymbol{M}_1$ describes the i, j pairwise interaction, and $\boldsymbol{A} = (A_{ij}) \in \mathbb{R}^{n\times n}$ captures the interacting structure between the oscillators. Although the systematic parameters $\boldsymbol{\mu}_{0,1}$ characterizing the dynamics $\boldsymbol{M}_{0,1}$ may be potentially distributed across the systems components, in this Letter we focus on the common $\boldsymbol{\mu}_{0,1}$ requiring that there exists a synchronous manifold $\mathcal{M} = \{\boldsymbol{x}_i = \boldsymbol{s},\ i = 1, \ldots, n\}$. We further require the coupling terms to be synchronization noninvasive, i.e., $\sum_{j=1}^{n} A_{ij}\boldsymbol{M}_1(\boldsymbol{s}, \boldsymbol{s}, \boldsymbol{\mu}_1) = \boldsymbol{0}$, which is satisfied when the interacting structure $\boldsymbol{A}$ is the Laplacian or the coupling function vanishes at the synchronous manifold $\boldsymbol{M}_1(\boldsymbol{s}, \boldsymbol{s}, \boldsymbol{\mu}_1) = \boldsymbol{0}$. We aim at designing only *noise controllers* such that (1) the network achieves the CS physically, that is, $\boldsymbol{x}_i(t) \to \mathcal{M}$ $(t \to +\infty)$ for all i, (2) the noise can act flexibly to any experimentally feasible parts of a system under consideration, including the parameters $\boldsymbol{\mu}_{0,1}$, the interacting structure $\boldsymbol{A}$, and the external forces, and (3) the controller adapts to practical requirements from the real-world

*Contact author: qxzhu16@fudan.edu.cn

†Contact author: wlin@fudan.edu.cn

scenarios, such as pinning control, communication constraints, and the common or uncorrelated noise.

AIN synchrony. For brevity of presentation, we succinctly denote the collective dynamics (1) as $\mathrm{d}\mathbf{x}/\mathrm{d}t = \boldsymbol{F}(\mathbf{x}, \boldsymbol{\mu})$ with $\mathbf{x} = (\boldsymbol{x}_i^\top, \ldots, \boldsymbol{x}_n^\top)^\top$ and $\boldsymbol{\mu} = \{\boldsymbol{\mu}_0, \boldsymbol{\mu}_1\}$. Consider the noise controlled variational dynamics of $\boldsymbol{\xi} = \mathbf{x} - \boldsymbol{E} \otimes \boldsymbol{s}$ with zero solution $\boldsymbol{\xi} \equiv \mathbf{0}$ as follows:

$$\begin{aligned}\mathrm{d}\boldsymbol{\xi} &= [\boldsymbol{F}(\boldsymbol{\xi} + \boldsymbol{E} \otimes \boldsymbol{s}, \boldsymbol{\mu}) - \boldsymbol{M}_0(\boldsymbol{s}, \boldsymbol{\mu}_0)]\mathrm{d}t + \boldsymbol{u}(\boldsymbol{\xi}, \boldsymbol{s})\mathrm{d}\boldsymbol{B}_t \\ &\triangleq \boldsymbol{G}(\boldsymbol{\xi}, \boldsymbol{s})\mathrm{d}t + \boldsymbol{u}(\boldsymbol{\xi}, \boldsymbol{s})\mathrm{d}\boldsymbol{B}_t, \end{aligned} \tag{2}$$

where $\boldsymbol{E} = (1, \ldots, 1)^\top \in \mathbb{R}^n$, $\otimes$ is the Kronecker product, $\boldsymbol{u} \in \mathbb{R}^{nd\times r}$ is the state-dependent stochastic controller, and $\boldsymbol{B}_t$ is the r-dimensional (rD) Brownian motion. The detailed formulation of how the noise controller acts on the parameters $\boldsymbol{\mu}$, the structure $\boldsymbol{A}$, and the external forces are provided in Sec. S1 in the Supplemental Material (SM) [22]. We propose the stability theory for devising the diffusion term $\boldsymbol{u}$ to stabilize the variational dynamics (2). The proof of this theory is included in SM-S2 [22].

Theorem 1. Suppose that there exists a function $V \in C^{1,2}(\mathbb{R} \times \mathbb{R}^{nd}; \mathbb{R}_{\geqslant 0})$ such that $V(\mathbf{0}, t) = 0$, $V(\boldsymbol{\xi}, t) \geqslant c\|\boldsymbol{\xi}\|^p$ for constants $c, p > 0$, and

$$\frac{[\nabla V(\boldsymbol{\xi}, t)^\top \boldsymbol{u}(\boldsymbol{\xi}, \boldsymbol{s})]^2}{V(\boldsymbol{\xi}, t)^2} - b \cdot \frac{\mathcal{L}V(\boldsymbol{\xi}, t)}{V(\boldsymbol{\xi}, t)} \geqslant 0, \quad \boldsymbol{\xi} \neq 0, \tag{3}$$

for some $b > 2$. Here, $\mathcal{L}$ represents Itô's derivative satisfying $\mathcal{L}V = V_t + \nabla V^\top \boldsymbol{G} + \mathrm{Tr}[\boldsymbol{u}^\top \nabla^2 V \boldsymbol{u}]/2$, ∇ represents the gradient operator with respect to $\boldsymbol{\xi}$, $\mathrm{Tr}[\cdot]$ represents the trace of a given matrix, and the limit $\lim_{\boldsymbol{x}\to\mathbf{0}} \frac{\|\nabla V(\boldsymbol{x},t)^\top \boldsymbol{u}(\boldsymbol{x},t)\|^2}{V(\boldsymbol{x},t)^2} > 0$ holds. Then, for $k > 0$, we obtain $\limsup_{t\to+\infty} \frac{1}{t}\ln\|\boldsymbol{\xi}(t)\| \leqslant -k\frac{b-2}{2bp}$ in a physical sense (i.e., with probability one).

Parametrization. Manually seeking the functions pair $V, \boldsymbol{u}$ satisfying the above conditions including (3) is *impractical* due to the complexity and nonlinearity of the original dynamics $\boldsymbol{G}$. To address this, we introduce the machine learning techniques and devise an algorithm that leverages $\boldsymbol{G}$ and $\boldsymbol{s}$ to identify the expected functions pair $V_{\boldsymbol{\theta}}$ and $\boldsymbol{u}_{\boldsymbol{\phi}}$, where $\boldsymbol{\theta}$ and $\boldsymbol{\phi}$ represent the parameters of the neural networks to be trained. To enhance training efficacy, we establish the neural networks such that $V_{\boldsymbol{\theta}}$ and $\boldsymbol{u}_{\boldsymbol{\phi}}$ meet specific prerequisites. Specifically, we construct the function $V_{\boldsymbol{\theta}}$ as $V_{\boldsymbol{\theta}}(\boldsymbol{\xi}, t) = \boldsymbol{g}_{\boldsymbol{\theta}}(\boldsymbol{\xi}, t) + \varepsilon\|\boldsymbol{\xi}\|^2$, where $\boldsymbol{g}_{\boldsymbol{\theta}}$ is a second-order differentiable input convex neural network [23,24] wherein $\boldsymbol{g}(\mathbf{0}, t) = 0$ and ε is a small hyperparameter guaranteeing the positive definite lower bound of $V_{\boldsymbol{\theta}}$. To proceed, we parametrize a synchronous-noninvasive controller with $\boldsymbol{u}_{\boldsymbol{\phi}}(\mathbf{0}) = \mathbf{0}$ and limit the Lipschitz constant of the controller using the spectral norm regularization method [25,26]. The detailed formulation of $V_{\boldsymbol{\theta}}$ and $\boldsymbol{u}_{\boldsymbol{\phi}}$ is provided in SM-S6. We theoretically validate the validity of the conditions assumed in Theorem 1 for the parametrized neural networks in SM-S2 [22].

Loss function. After parametrizing $V_{\boldsymbol{\theta}}$ and $\boldsymbol{u}_{\boldsymbol{\phi}}$, we need to ensure the controlled variational dynamics (2) satisfying the conditions established in (3). As such, we can attain the CS in the original collective dynamics (1) under noise control. To do so, we heuristically devise the loss function as $L(\boldsymbol{\theta}, \boldsymbol{\phi}) = \frac{1}{m}\sum_{i=1}^{m}\{\frac{b\cdot\mathcal{L}V_{\boldsymbol{\theta}}(\boldsymbol{\xi}_i,t_i)}{V_{\boldsymbol{\theta}}(\boldsymbol{\xi}_i,t_i)} - \frac{[\nabla V_{\boldsymbol{\theta}}(\boldsymbol{\xi}_i,t_i)^\top \boldsymbol{u}_{\boldsymbol{\phi}}(\boldsymbol{\xi}_i,\boldsymbol{s}(t_i))]^2}{V_{\boldsymbol{\theta}}(\boldsymbol{\xi}_i,t_i)^2}\}^+$, where $\{\boldsymbol{\xi}_i, \boldsymbol{s}(t_i), t_i\}_{i=1}^m$ is the training data set and $\{\cdot\}^+$ denotes the operation of $\max(0, \cdot)$. To circumvent the drawback that training on the finite data set may not guarantee the validity of the stability condition in Eq. (3) on the whole space, we further provide a stability guarantee theory to endow the stability guarantee to the current framework (for more details refer to SM-S2 [22]).

Theorem 2. With the functions specified in Theorem 1, we denote by M the maximal Lipschitz constant of $\|\nabla V^\top \boldsymbol{u}\|^2$ and $\mathcal{L}V \cdot V$ on $\mathcal{D}$, where $\mathcal{D}$ is a bounded state space. Further we denote by $\tilde{\mathcal{D}}$ the finite discretization of $\mathcal{D}$ with size r such that, for each $\boldsymbol{x} \in \mathcal{D}$, there exists $\tilde{\boldsymbol{x}} \in \tilde{\mathcal{D}}$ with $\|\boldsymbol{x} - \tilde{\boldsymbol{x}}\| < r$. If there exists a constant $0 \leqslant \delta \leqslant Mr$ such that $-\|\nabla V(\tilde{\boldsymbol{x}}, t)^\top \boldsymbol{u}(\tilde{\boldsymbol{x}}, t)\|^2 + b \cdot \mathcal{L}V(\tilde{\boldsymbol{x}}, t)V(\tilde{\boldsymbol{x}}, t) + (2 + b)Mr \leqslant \delta$ for all $\tilde{\boldsymbol{x}} \in \tilde{\mathcal{D}}\backslash\{\mathbf{0}\}$, then the controller $\boldsymbol{u}$ rigorously satisfies the stability condition in Eq. (3). Therefore, the learned noise controller rigorously satisfies the stability condition through replacing the training data set by $\tilde{\mathcal{D}}$ and slightly modifying the loss function with the newly added term $(2 + b)Mr$.

Accelerating the training process. The computational cost for computing the Hessian matrix in $\mathrm{Tr}[\boldsymbol{u}^\top \nabla^2 V_{\boldsymbol{\theta}} \boldsymbol{u}]$ is $\mathcal{O}(d^2)$, which hinders the framework from scaling to higher dimensional tasks. To reduce the computational cost, we establish an unbiased estimator as $\mathrm{Tr}[\boldsymbol{u}^\top \nabla^2 V_{\boldsymbol{\theta}} \boldsymbol{u}] = \mathbb{E}[(\nabla(\boldsymbol{\eta}^\top \nabla V_{\boldsymbol{\theta}}))^\top \boldsymbol{u}\boldsymbol{u}^\top \boldsymbol{\eta}]$, where $\boldsymbol{\eta}$ is a dD noise vector with zero means, commonly referred to as Hutchinson's trace estimator [27]. We thus substitute this expectation representation with the Monte Carlo estimator, so that $\mathrm{Tr}[\boldsymbol{u}^\top \nabla^2 V_{\boldsymbol{\theta}} \boldsymbol{u}] \approx \frac{1}{m}\sum_{i=1}^{m}(\nabla(\boldsymbol{\eta}_i^\top \nabla V_{\boldsymbol{\theta}}))^\top \boldsymbol{u}\boldsymbol{u}^\top \boldsymbol{\eta}_i$ with m noise vectors during our training process. This approach reduces the computational cost from $\mathcal{O}(d^2)$ to $\mathcal{O}(md)$, improving the efficiency of the AIN synchrony in the higher dimensional task, especially for $m \ll d$.

Except for considering the ground-truth variational dynamics (2), we can also apply the above-established machine learning framework to the traditional linearization equations $\mathrm{d}\boldsymbol{\xi}/\mathrm{d}t = [\boldsymbol{I}_n \otimes \nabla \boldsymbol{M}_0 + \boldsymbol{A} \otimes \nabla \boldsymbol{M}_1]\boldsymbol{\xi}$, which find extensive application in the master stability function theories for realizing CS [28,29] (see SM-S3). In addition, as suggested by the stabilization theory, our framework can also be extended to the nonautonomous dynamics, such as the coupling matrix $\boldsymbol{A} = \boldsymbol{A}(t)$ varying temporally (see SM-S4 and SM-S6.4 [22]).

To proceed, we numerically validate the efficacy and flexibility of the AIN synchrony using several representative physical models under the realistic constraints.

AIN synchrony for driving-response Lorenz systems. We investigate the unidirectionally coupled Lorenz systems, where the driving and the response systems, respectively, are $\mathrm{d}\boldsymbol{x}_1/\mathrm{d}t = \boldsymbol{f}(\boldsymbol{x}_1, \sigma, \rho, \beta)$ and $\mathrm{d}\boldsymbol{x}_2 = \boldsymbol{f}(\boldsymbol{x}_2, \sigma, \rho, \beta) + \boldsymbol{u}(\boldsymbol{\xi}, \boldsymbol{x}_1)\mathrm{d}B_t$ with $\boldsymbol{x}_i = (x_i, y_i, z_i)^\top$, $\boldsymbol{\xi} = (\xi_1, \xi_2, \xi_3)^\top = (x_1 - x_2, y_1 - y_2, z_1 - z_2)^\top$, $\boldsymbol{f}(\boldsymbol{x}_i, \sigma, \rho, \beta) = [\sigma(y_i - x_i), \rho x_i - y_i - x_i z_i, x_i y_i - \beta z_i]^\top$, and $i = 1, 2$. The Lorenz system is characterized by three parameters σ, ρ, β, being proportional to the Prandtl number, the Rayleigh number, and certain physical dimensions of the layer itself, respectively, which are all experimentally adjustable [30]. In addition, we apply the *pinning control* on this system by partially controlling some variables of the system. As shown in Fig. 1(a), we explore both the parameters control and the

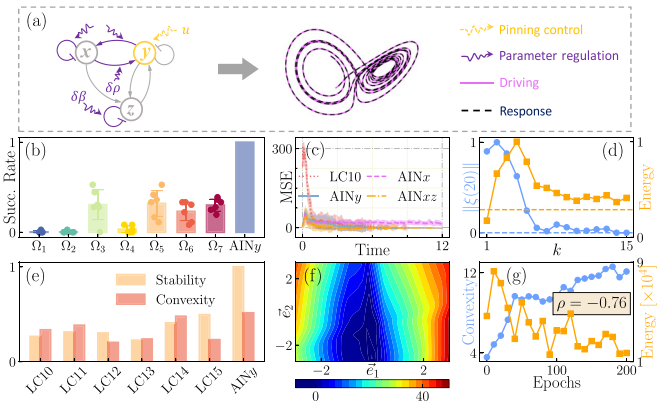

FIG. 1. Synchronizing the driving-response Lorenz systems. (a) Sketch on different noise controlling modes by the parameter regulation and by the external forces. (b) The success rate of seven combinations of the regulated parameters, compared with the pinning controller AINy. The dots in the left seven bars represent the success rate with $\boldsymbol{u}_{\max} \in \{1.0, 1.2, 1.4, 1.6, 1.8, 2.0\}$, where $\boldsymbol{u}_{\max} = \max_{\boldsymbol{x}} \|\boldsymbol{u}(\boldsymbol{x})\|_\infty$. (c) The MSE between the driving and the response systems under different controllers with the shaded region representing the variance. (d) The synchronization error (blue circle) at time 20 and the energy cost (orange square) in the controlling process against the strength of the linear controller. The horizontal dashed lines represent the corresponding values of the learned controller AINy. (e) The stability (left bar) of the controlled trajectories and the convexity (right bar) of the learned V function of linear controllers compared with that of AINy. (f) The projection of $V_{\text{AIN}y} - V_{\text{LC}_{10}}$ to a random selected 2D section. (g) The convexity (blue circle) of the V function for the AINy and the energy cost (orange square) over the training process, and their Pearson correlation coefficient ρ.

pinning control for synchronizing the response system to the attractor produced by the driving Lorenz system. First, we study whether the CS of the driving-response systems is achieved by solely regulating the parameters of the response system using noise. For instance, we examine the impact of adjusting the Prandtl number with noise, employing $\boldsymbol{u} = [\delta\sigma(\boldsymbol{\xi})(y_2 - x_2), 0, 0]^\top$ with $\delta\sigma(\boldsymbol{0}) = 0$ as the controller. We employ a loss function after training and the temporal average of the mean square error (MSE) between the driving system and the coupled response system as indicators to evaluate the controller performance. We consider totally seven different combinations of the controlled parameters, including $\Omega_1 = \{\sigma\}$, $\Omega_2 = \{\rho\}$, $\Omega_3 = \{\beta\}$, $\Omega_4 = \{\sigma, \rho\}$, $\Omega_5 = \{\sigma, \beta\}$, $\Omega_6 = \{\rho, \beta\}$, and $\Omega_7 = \{\sigma, \rho, \beta\}$, with a requirement for the scale of the learned noise $\boldsymbol{u}_{\max}$ to be less than 2 for realizing feasible simulations. In Fig. 1(b), we compare $\Omega_{1:7}$ with another pinning controller in the rate of successfully synchronizing the driving-response systems over 50 samples. The results indicate that the parameter β dominates the behavior of the Lorenz system among all these three parameters. Moreover, the findings imply that parameter regulation with noise is not always as effective as external forces, which agrees with the intuition.

Next, we delve into the intricacies of the task of pinning control. Initially, our focus centers on the pinning controllers that act on the nodes x_2 and y_2, denoted by AINx and AINy, respectively. As shown in Fig. 1(c), AINy succeeds in this task while AINx does not; this implies that node y exerts greater influence on the whole dynamics compared to the node x in the Lorenz system in the presence of the noise controller. Additionally, we identify the pinning controller on both x and z, denoted by AINxz, as efficacious. Furthermore, we compare the AINy with the stochastic linear controllers LCk, i.e., $\boldsymbol{u} = [0, k(\xi_1 + \xi_2 + \xi_3), 0]^\top$, that only acts on y_2 using different strengths k $(= 1, \ldots, 15)$, in terms of the MSE and the energy cost [we also try the linear controller $\boldsymbol{u} = (0, k\xi_2, 0)^\top$, but it fails to synchronize the system for any strength k; see Sec. S6.1 of SM for more detailed discussion [22]]. Figure 1(d) reveals that the AINy is significantly more energy saving than the linear LCk for $k \geqslant 6$ that successfully synchronizes the driving-response systems, hinting an *implicit energy regularization* in the AIN synchrony. To gain more insights into the observed implicit energy regularization, we focus on the linear controller LCk and train $V_{\boldsymbol{\theta}_k}$ for each LCk within our framework. We consider the spatial convexity $\mathbb{E}_{\boldsymbol{\xi}}[\frac{1}{nd}\sum_{i=1}^{nd}\lambda_i(\nabla^2 V)]$ defined by the eigenvalues of the Hessian matrix of V. Numerical comparisons of the spatial convexity of $V_{\boldsymbol{\theta}_k}$ and $V_{\boldsymbol{\theta}_{\text{AIN}y}}$ are presented in Fig. 1(e), revealing that the $V_{\boldsymbol{\theta}_{\text{AIN}y}}$ function of the AINy boasts the greatest convexity among successful controllers. This finding is further demonstrated in Fig. 1(f), where the random projection onto the 2D surface of the section of $V_{\boldsymbol{\theta}_{\text{AIN}y}} - V_{\boldsymbol{\theta}_{\text{LC}10}}$ exhibits a pronounced steepness. Figure 1(g) shows the anticorrelation between the energy cost and the convexity of V in the training process, which validates the implicit energy regularization from the numerical perspective. Furthermore, the following theorem elucidates the mechanism of these findings.

Theorem 3. Consider the controlled dynamics in (2) with the AIN synchrony controller $\boldsymbol{u}_{\boldsymbol{\phi}}$ learned according to the stability condition in Eq. (3). Then, the loss function in the training process is equivalent to the control energy in the control process by norm, $E = \mathbb{E}\int_0^T \|\boldsymbol{u}_{\boldsymbol{\phi}}^\top(\boldsymbol{x}(t), \boldsymbol{s}(t))Q\boldsymbol{u}_{\boldsymbol{\phi}}(\boldsymbol{x}(t), \boldsymbol{s}(t))\|\mathrm{d}t$, where Q is the variance matrix of the Brownian motion.

Consequently, as we minimize the loss function, the control energy is optimized as well, which thus results in the implicit energy regularization. More detailed demonstrations are included in SM-S5 [22].

AIN synchrony for subcritical Landau-Stuart oscillator. Consider coupled Landau-Stuart oscillators governed by the complex-valued differential equations: $\dot{Z}_j = (\beta + \mathrm{i}\gamma + \mu|Z_j|^2)Z_j + \sum_{k=1}^n A_{jk}Z_k$ for $Z_j \in \mathbb{C}$, $j = 1, \ldots, n$, $\beta < 0$, and $\mu > 0$. Here, the self-dynamics undergoing the subcritical Andronov-Hopf bifurcation possesses an unstable periodic orbit (UPO) [31]. We focus on synchronizing the coupled oscillators to the UPO under several typical communication constraints, e.g., (i) all oscillators communicate, (ii) half of the oscillators communicate, and (iii) none of the oscillators communicate (resulting in a decentralized controller), as shown in Fig. 2(a).

We examine the impact of communication constraints on the energy cost, the success rate of stabilization and synchronization, the transient time from initial values to the synchronization manifold on the UPO, and the stability of the controllers. We utilize the order parameter $R_1 = \frac{1}{n}\sum_{j=1}^n e^{\mathrm{i}\theta_j}$ as the synchronization indicator, where θ_j is the argument of

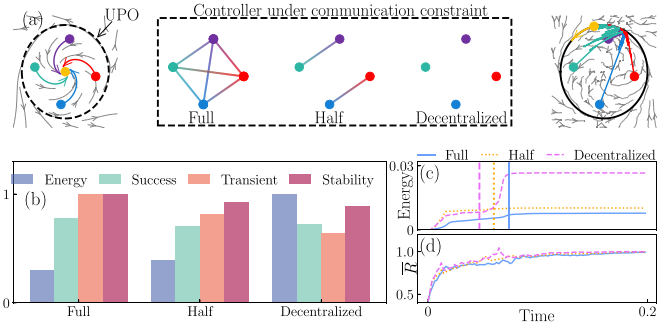

FIG. 2. Synchronizing the subcritical Landau-Stuart oscillators under different communication constraints. (a) Illustration of the CS task. (b) From left to right are bar plots of energy cost, succeeding rate, transient time $\tau_{0.1}$, and stability at three different communication modes for 50 sample trajectories and the mean first passage time $\tau_{0.1}$ of the controlled process. All the indices are normalized to $[0, 1]$. (c) Energy cost and (d) success indicator $\overline{R}$ with time, where the vertical lines represent the corresponding values of $\tau_{0.1}$.

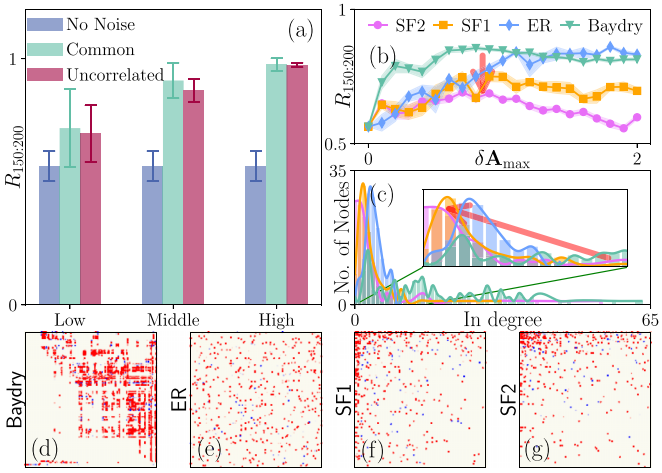

FIG. 3. Synchronizing the coupled FitzHigh-Nagumo oscillators on four respective networks. (a) The order parameter R in the time interval [150,200] under external stochastic forces at three different types of noise intensities: low ($\boldsymbol{u}_{\max} = 1.0$), middle ($\boldsymbol{u}_{\max} = 1.5$), and high ($\boldsymbol{u}_{\max} = 2.0$), for 10 realizations in each type of noise. Error bars indicate the variance. The bars corresponding to no noise, common noise, and uncorrelated noise are shown from left to right in order. (b) $R_{150:200}$ of the noise perturbed system using the respective networks over the weight perturbed strength $\boldsymbol{\delta A}_{\max} \in [0, 2]$. (c) The in-degree distribution of the four networks, where the inset panel shows the difference among the peaks and the flatnesses of these networks. (d)–(g) The heat maps of the learned optimal weighted perturbation structure.

the complex variable Z_j. Additionally, we employ the distance $R_2 = \frac{1}{n}\sum_{j=1}^{n} |Z_j|$ between the UPO and the controlled orbits as the stabilization indicator. We set $\overline{R} = (R_1 + R_2)/2$ as the success indicator and the transient time is assessed by the empirical expectation of the stopping time $\tau_p = \inf\{t \geqslant 0 : 1 - |\overline{R}(t)| = p\} \vee \inf\{t \geqslant 0 : |\overline{R}(t)| = 1 - p\}$ over the trajectories with a predefined accuracy p. The stability of the controllers is captured by the reciprocal empirical average of the standard variance of the trajectories. The results are comprehensively presented in Fig. 2(b). Although there is no significant difference in success rate and stability, we observed an interesting trade-off phenomenon that the energy cost increases with the decreased communication capability while the transient time decreases. This property is further demonstrated in Figs. 2(c) and 2(d). The reason is that full communication optimally allocates control resources, achieving the task with smaller control costs. As a result, the reduced energy leads to the prolonged transient time since they have significant anticorrelation.

AIN synchrony for networked neuronal dynamics. Finally, we synchronize the higher-dimensional networked dynamics using the coupled FitzHugh-Nagumo (FHN) neuronal oscillators with two modes of artificial noise, including direct driving force on each node and perturbing the coupling structure. The networked neuronal dynamics are described by $\mathrm{d}v_i/\mathrm{d}t = (v_i - v_i^3/3 - w_i) + \sum_{j=1}^{n} L_{ij}/(1 + e^{-10v_j})$ and $\mathrm{d}w_i/\mathrm{d}t = 0.1(v_i + 0.7 - 0.8w_i)$, where $(L_{ij})_{n\times n} = (\delta_{ij}\sum_{j=1}^{n} A_{ij} - A_{ij})_{n\times n}$ is the Laplacian matrix of coupling matrix $\boldsymbol{A} = (A_{ij})_{n\times n}$ [32–34]. To quantify the synchronization of all the FHN oscillators, we employ the order parameter introduced in [35] as $R = \frac{\langle M^2\rangle - \langle M\rangle^2}{\frac{1}{N}\sum_{i=1}^{N}(\langle v_i^2\rangle - \langle v_i\rangle^2)}$, where $M = \frac{1}{N}\sum_{i=1}^{N} v_i$ is the mean field and $\langle\cdot\rangle$ represents the time average. As such, $R = 0$ corresponds to the asynchronous regime, while $R = 1$ indicates the CS state. For the external noise forces, we compare the effects of the *common* noise and the *uncorrelated* noise under different noise intensities in achieving the CS; we employ the Baydry, a realistic foodweb network [36] with $n = 128$. As shown in Fig. 3(a), common noise gets a larger order parameter while uncorrelated noise exhibits smaller variance over multiple realizations in all noise scales, forming an interesting trade-off between performance and robustness. In the latter control mode, we perturb the structure with $\boldsymbol{\delta A}$ driven by the Brownian motion (see Table S1 in SM-S1 for the detailed formulation [22]). We investigate the influence of network structure using four coupling matrices, viz., the Baydry, the directed Erdös and Rényi (ER) network, and two scale-free networks (denoted by SF1 and SF2) [37]. Figure 3(b) shows the order parameter of the noise-perturbed dynamics under four networks against the perturbation intensity $\boldsymbol{\delta A}_{\max} = \|\boldsymbol{\delta A}\|_\infty$. The CS performance of the realistic network significantly exceeds the others in the low intensity. As the intensity increases, the ER network outperforms the Baydry foodweb slightly, and both outperform SF1, with SF1 surpassing SF2. To uncover the mechanism behind this phenomenon, we analyze the in-degree distribution plotted in Fig. 3(c). We find that the distribution of the Baydry foodweb is the most flat, having a heavy tail, while the peaks of the distributions ER, SF1, and SF2 tend towards zero. This indicates that the impact of noise decreases gradually as the homogeneity of the networks grows, as further demonstrated in Figs. 3(d)–3(g).

Conclusion. We have conceived and formulated a machine learning framework to artificially generate noise controllers for synchronizing both general chaotic systems and limit-cycle systems. Harnessing the commutation property of the trace estimator, our framework scales to any higher dimensional systems with a linear-order computational cost.

We applied our AIN synchrony framework to successfully synchronize several representative systems under different constraints conforming to realistic scenarios. The results reveal that the machine-learning-coined noise has an implicit energy regularization phenomenon, inducing the energy-saving synchrony. Furthermore, a further generalization of our current framework is anticipated to the situation where a more general form of noise [38] is taken into account.

Acknowledgments. W.L. is supported by the NSFC (Grant No. 11925103), the IPSMEC (Grant No. 2023ZKZD04), and the STCSM (Grants No. 22JC1401402, No. 22JC1402500, and No. 2021SHZDZX0103). Q.Z. is supported by the China Postdoctoral Science Foundation (Grant No. 2022M720817), by the Shanghai Postdoctoral Excellence Program (Grant No. 2021091), and by the STCSM (Grants No. 21511100200, No. 22ZR1407300, and No. 23YF1402500).

[1] H. Nakao, K. Arai, and Y. Kawamura, Phys. Rev. Lett. **98**, 184101 (2007).
[2] R. F. Galán, N. Fourcaud-Trocmé, G. B. Ermentrout, and N. N. Urban, J. Neurosci. **26**, 3646 (2006).
[3] R. V. Jensen, Phys. Rev. E **58**, R6907 (1998).
[4] C.-H. Lai and C. Zhou, Europhys. Lett. **43**, 376 (1998).
[5] L. Gammaitoni, P. Hänggi, P. Jung, and F. Marchesoni, Rev. Mod. Phys. **70**, 223 (1998).
[6] C. Zhou and J. Kurths, Chaos **13**, 401 (2003).
[7] J.-N. Teramae and D. Tanaka, Phys. Rev. Lett. **93**, 204103 (2004).
[8] C. Zhou and J. Kurths, Phys. Rev. Lett. **88**, 230602 (2002).
[9] C. Zhou, J. Kurths, I. Z. Kiss, and J. L. Hudson, Phys. Rev. Lett. **89**, 014101 (2002).
[10] W. Lin and G. Chen, Chaos **16**, 013134 (2006).
[11] S. Zhou, Y. Guo, M. Liu, Y.-C. Lai, and W. Lin, Phys. Rev. E **100**, 032302 (2019).
[12] S. Zhou, W. Lin, and J. Wu, Automatica **143**, 110436 (2022).
[13] A. Maritan and J. R. Banavar, Phys. Rev. Lett. **72**, 1451 (1994).
[14] R. Toral, C. R. Mirasso, E. Hernández-Garcıa, and O. Piro, Chaos **11**, 665 (2001).
[15] A. S. Pikovsky, Phys. Rev. Lett. **73**, 2931 (1994).
[16] J. H. Meng and H. Riecke, Sci. Rep. **8**, 6949 (2018).
[17] S. Martineau, T. Saffold, T. T. Chang, and H. Ronellenfitsch, Phys. Rev. Lett. **128**, 098301 (2022).
[18] S. Boccaletti, J. Kurths, G. Osipov, D. Valladares, and C. Zhou, Phys. Rep. **366**, 1 (2002).
[19] S. Zhou, Y.-C. Lai, and W. Lin, SIAM J. Appl. Dyn. Syst. **21**, 932 (2022).
[20] S. Zhou, W. Lin, X. Mao, and J. Wu, IEEE Trans. Automat. Contr. **69**, 85 (2023).
[21] X. Peng and S. Zhou, Syst. Contr. Lett. **184**, 105711 (2024).
[22] See Supplemental Material at http://link.aps.org/supplemental/10.1103/PhysRevE.110.L012203 for the detailed formulation of the flexible noise control, the stochastic stabilization theory for the AIN control, the results on controlling linear variational equations and temporal networks, the implicit energy regularization theory, the simulation configurations, and the perspective of the present work, which includes Refs. [37,39–63].
[23] J. Zhang, Q. Zhu, and W. Lin, *Advances in Neural Information Processing Systems* (Curran Associates, Inc., New York, 2022), Vol. 35, pp. 9098–9110.
[24] J. Zhang, L. Yang, Q. Zhu, and W. Lin, *International Conference on Machine Learning* (ACM, New York, 2024).
[25] J. Zhang, Q. Zhu, W. Yang, and W. Lin, *International Conference on Learning Representations* (OpenReview, Kigali, 2023).
[26] Y. Yoshida and T. Miyato, arXiv:1705.10941.
[27] M. F. Hutchinson, Commun. Stat. Simul. Comput. **18**, 1059 (1989).
[28] L. M. Pecora and T. L. Carroll, Phys. Rev. Lett. **80**, 2109 (1998).
[29] A. Ghosh, H. Behl, E. Dupont, P. Torr, and V. Namboodiri, *Advances in Neural Information Processing Systems* (Curran Associates, Inc., New York, 2020), Vol. 33, pp. 14831–14843.
[30] M. Gorman, P. Widmann, and K. Robbins, Physica D **19**, 255 (1986).
[31] Y. A. Kuznetsov, Scholarpedia **1**, 1858 (2006).
[32] K. Wang, L. Yang, S. Zhou, and W. Lin, Chaos **33**, 091101 (2023).
[33] C. Conley and J. Smoller, J. Diff. Eq. **63**, 389 (1986).
[34] J. Keener and J. Sneyd, *Mathematical Physiology* (Springer-Verlag, New York, 1998).
[35] J. Garcia-Ojalvo, M. B. Elowitz, and S. H. Strogatz, Proc. Natl. Acad. Sci. USA **101**, 10955 (2004).
[36] Y.-Z. Sun, S.-Y. Leng, Y.-C. Lai, C. Grebogi, and W. Lin, Phys. Rev. Lett. **119**, 198301 (2017).
[37] K.-I. Goh, B. Kahng, and D. Kim, Phys. Rev. Lett. **87**, 278701 (2001).
[38] X. Peng, S. Zhou, W. Lin, and X. Mao, SIAM J. Control Optim. **62**, 1569 (2024).
[39] W. Yu, G. Chen, J. Lu, and J. Kurths, SIAM J. Control Optim. **51**, 1395 (2013).
[40] W. Cui, Y. Jiang, B. Zhang, and Y. Shi, *Advances in Neural Information Processing Systems* (Curran Associates, Inc., Red Hook, NY, 2024), Vol. 36.
[41] Y. Zhang and S. H. Strogatz, Nat. Commun. **12**, 3273 (2021).
[42] X. Mao, *Stochastic Differential Equations And Applications* (Elsevier, Amsterdam, 2007).
[43] B. Oksendal, *Stochastic Differential Equations: An Introduction With Applications* (Springer Science & Business Media, New York, 2013).
[44] K. L. Chung and P. Erdös, Trans. Amer. Math. Soc. **72**, 179 (1952).
[45] B. Amos, L. Xu, and J. Z. Kolter, *International Conference on Machine Learning* (ACM, New York, 2017), pp. 146–155.
[46] T. Miyato, T. Kataoka, M. Koyama, and Y. Yoshida, *International Conference on Learning Representations* (OpenReview, Vancouver, 2018).
[47] H. Gouk, E. Frank, B. Pfahringer, and M. J. Cree, Mach. Learn. **110**, 393 (2021).
[48] H.-T. D. Liu, F. Williams, A. Jacobson, S. Fidler, and O. Litany, *Special Interest Group on Computer Graphics and Interactive Techniques Conference Proceedings* (ACM, New York, 2022), pp. 1–13.

[49] T. Yamada, J. Math. Kyot. Univ. **13**, 497 (1973).
[50] V. I. Arnold, *Ordinary Differential Equations* (Springer Science & Business Media, New York, 1992).
[51] S. Lang, *Algebra* (Springer Science & Business Media, New York, 2012), Vol. 211.
[52] A. Paszke, S. Gross, F. Massa, A. Lerer, J. Bradbury, G. Chanan, T. Killeen, Z. Lin, N. Gimelshein, L. Antiga *et al.*, *Advances in Neural Information Processing Systems* (Curran Associates, Inc., New York, 2019), Vol. 32, pp. 8026–8037.
[53] D. P. Kingma and J. Ba, arXiv:1412.6980.
[54] W. Grathwohl, R. T. Chen, J. Bettencourt, I. Sutskever, and D. Duvenaud, *International Conference on Learning Representations* (OpenReview, Vancouver, 2018).
[55] Y. Song, S. Garg, J. Shi, and S. Ermon, *Uncertainty in Artificial Intelligence* (ACM, New York, 2020), pp. 574–584.
[56] R. T. Chen, Y. Rubanova, J. Bettencourt, and D. K. Duvenaud, *Advances in Neural Information Processing Systems* (Curran Associates, Inc., New York, 2018), Vol. 31, pp. 6571–6583.
[57] J. Li, X. Li, and S. Liao, Research square (2020), https://doi.org/10.21203/rs.3.rs-49069/v1.
[58] P. Erdős, A. Rényi *et al.*, Publ. Math. Inst. Hung. Acad. Sci. **5**, 17 (1960).
[59] P. De Lellis, M. Di Bernardo, and F. Garofalo, Chaos **18**, 037110 (2008).
[60] X. F. Wang and G. Chen, Physica A **310**, 521 (2002).
[61] J. Lu, J. Kurths, J. Cao, N. Mahdavi, and C. Huang, IEEE Trans. Neural Netw. Learn. Syst. **23**, 285 (2011).
[62] T. Chen, X. Liu, and W. Lu, IEEE Trans. Circuits Syst. I **54**, 1317 (2007).
[63] C.-C. Wang, E. L. Lloyd, and M. L. Soffa, J. ACM **32**, 296 (1985).